Analysis of combined moire and laser speckle grating methods used in 3-D crack tip deformation measurements

Hareesh V. Tippur and Fu-Pen Chiang

The paper provides analyses for two optical schemes developed for mapping 3-D crack tip fields in ductile materials. The first scheme combines the in-plane moire method with the projection moire method to determine all three displacement components simultaneously. In the second method, we combined one-beam laser speckle photography with the projection moire method to measure 3-D deformation fields. The experimental results obtained using these methods are presented.

I. Introduction

The measurement of field parameters in the immediate vicinity of a crack tip is of interest in most fracture studies. Due to the 3-D nature of the displacement field surrounding the crack tip vicinity, the experimental method used must have the potential to measure simultaneously all three displacement components. Existing experimental techniques used in fracture investigations, such as photoelasticity, moire methods,[1] laser speckle interferometry,[2] and holography, are convenient for making either in-plane or out-of-plane measurements alone. The method of caustics[3,4] provides information about stress intensification at the crack tip using the derivatives of out-of-plane displacement. However, it requires that one know *a priori* the nature of the out-of-plane displacement field.

There is a need for experimental methods which can directly measure all three deformation components for a better understanding of the crack tip behavior. Optical techniques used in experimental fracture mechanics provide either in-plane or out-of-plane deformation information. Complete 3-D deformation measurement requires combining some of the existing procedures. In the past, there have been a few attempts in this direction. Adams and Maddux[5] combined image plane holography with laser speckle photography to obtain in-plane and out-of-plane displacements from a holospecklegram. Chiang *et al.*[6] have used Fourier plane holography with speckle photography. Wu and Chiang[7] used a sandwich holography technique for measuring 3-D displacement fields near the blunt notch in a three-point bend specimen. Jaisingh[8] used laser speckle photography with projection moire[9] to measure elastic displacements of a cantilever beam. Chiang and Williams[10] have measured residual displacements ahead of a plastically deformed elliptical cutout in a tensile strip using a combination of in-plane moire and shadow moire methods.

We present the analyses for two methods, namely, the combined moire method and the laser speckle grating method useful in measuring 3-D deformation fields near plastically deformed cracks. The approach is an offshoot of the previous works of Jaisingh[8] and Chiang and Williams.[10] First-order analyses pertaining to recording and spatial filtering steps are provided for both methods.

II. Combined Moire Method

The combined moire method couples the in-plane moire method for mapping in-plane displacements with the projection moire method for out-of-plane displacement mapping. Here the specimen surface is photoprinted with a high density dot pattern with its principal directions parallel to the Cartesian coordinates ξ_1 (or x_1) and ξ_2 (or x_2). Onto this specimen surface, a line grating is projected with a projection angle β. The grating projection is done as follows (Fig. 1): A He–Ne laser beam is first expanded by a microscopic objective and then collimated by a field lens before it impinges on a line grating. The regular and diffracted wavefronts are collected by a second field lens which forms the diffraction spectrum of the grat-

Hareesh Tippur is with Auburn University, Department of Mechanical Engineering, Auburn, Alabama 36849-5341, and F. P. Chiang is with State University of New York at Stony Brook, Laboratory for Experimental Mechanics Research, Stony Brook, New York 11794-2300.

Received 10 October 1988.
0003-6935/91/192748-09$05.00/0.

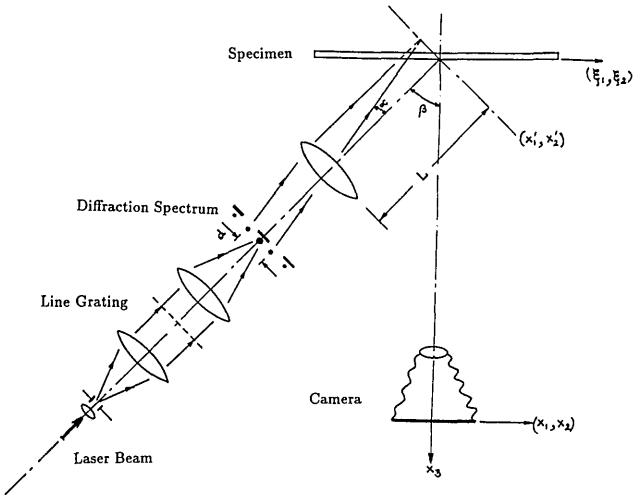

Fig. 1. Schematic of the experimental arrangement for projecting gratings on the specimen surface. The specimen surface is photoprinted with cross gratings in the combined moire method and is coated with a mist of flat white paint in the laser speckle grating method.

ing at its focal plane in the form of a series of equally spaced bright spots called diffraction orders. All the orders are blocked out by a mask except the ±1 which is collected by a third field lens to form two nearly collimated beams with an angle 2α between them to impinge on the specimen. Within these intersecting beams there exists a standing wave of period (or pitch) ρ_0:

$$\rho_0 = \frac{\lambda}{2\sin\alpha}, \tag{1}$$

where λ is the wavelength of light. Due to the angular projection parameter β of the setup, the pitch of the grating on the specimen surface is

$$\rho = \frac{\lambda}{2\sin\alpha\cos\beta}, \tag{2}$$

The formation of the projected grating (or standing wave) is explained as follows: the light intensity distribution on $x_1'x_2'$ plane is

$$I_g(x_1',x_2') = a_{+1}^2 + a_{-1}^2 + 2a_{+1}a_{-1}\cos\delta, \tag{3}$$

where a_{+1} and a_{-1} are light amplitudes of +1 and −1 diffraction orders and δ represents the path difference between them. Hence

$$\delta = \frac{2\pi}{\lambda} d\sin\alpha, \tag{4}$$

where d is the distance between the two diffraction orders. Since the amplitudes of ±1 diffraction orders are the same (or $a_{+1} = a_{-1} = a$) and intensity I_g is maximum when $\delta = 2n\pi$ or $d\sin\alpha = n\lambda$, where $n = 0,1,2,\ldots$. Noting that $\sin\alpha \approx x_1'/L$,

$$I_g(x_1',x_2') = 2a^2\left(1 + \cos\frac{2\pi d x_1'}{\lambda L}\right), \tag{5}$$

$$I_g(\xi_1,\xi_2) = 2a^2\left(1 + \cos\frac{2\pi\xi_1 d\cos\beta}{\lambda L}\right) = 2a^2\left(1 + \cos\frac{2\pi\xi_1}{\rho}\right). \tag{6}$$

Or, the intensity on the image plane for the magnification factor = 1 is

$$I_g(x_1,x_2) = 2a^2\left(1 + \cos\frac{2\pi x_1}{\rho}\right), \tag{7}$$

where ρ is the pitch of the projected grating.

When the specimen deforms due to the applied loads, the photoprinted cross grating deforms according to the in-plane displacements (components u_1 along x_1 and u_2 along x_2), whereas projected gratings follow out-of-plane displacements (u_3 along x_3). All three gratings are recorded on high contrast films by a single exposure as a master (when the load is zero) and deformed gratings. An enlargement of a typical combined grating recording is shown in Fig. 2(a). On superposing the master grating with a deformed grating, all the fringe patterns corresponding to u_1,u_2, and u_3 displacements can be obtained. To delineate each of these contour maps from the other two, optical spatial filtering[11] is performed. The schematic of optical spatial filtering is shown in Fig. 2(b). The process of spatial filtering and fringe formation can be described as follows.

For the sake of mathematical simplicity, let us assume that the recorded gratings have sinusoidal transmittance. Without losing generality, let the gratings be recorded with a magnification factor equal to 1. The transmittance of a single grating of pitch p and x_1 as its principal direction can be expressed as

$$t = \left(1 + \cos\frac{2\pi x_1}{p}\right). \tag{8}$$

In the combined moire method, there are three such gratings with different pitch and principal directions. Thus the transmittance of an undeformed grating obtained from the combined moire method can be approximated by

$$t_g = \left(1 + \cos\frac{2\pi x_1}{p}\right)\left(1 + \cos\frac{2\pi x_2}{q}\right)\left(1 + \cos\frac{2\pi x_1}{\rho}\right), \tag{9}$$

where p and q are the pitch of the photoprinted undeformed gratings along the x_1- and x_2-directions. The undeformed projected grating has a pitch ρ ($>p$), and its principal direction is parallel to the x_1-axis. After deformation, the grating pitches change to p', q', and ρ', respectively, where $p' = p + \Delta p(x_1,x_2)$, $q' = q + \Delta q(x_1,x_2)$, and $\rho' = \rho + \Delta\rho(x_1,x_2)$. Thus transmittance of a deformed grating is

$$t_g' = \left(1 + \cos\frac{2\pi x_1}{p'}\right)\left(1 + \cos\frac{2\pi x_2}{q'}\right)\left(1 + \cos\frac{2\pi x_1}{\rho'}\right). \tag{10}$$

Spatial filtering is performed to delineate individual deformation fields, and the Fourier transform properties of thin lenses are incorporated in the analysis. It is also assumed that Δp, Δq, and $\Delta\rho$ are slowly varying functions of the in-plane coordinates x_1,x_2. Hence

$$FT[t_g t_{g'}] = T_g(r_1,r_2) \otimes T_{g'}(r_1,r_2), \tag{11}$$

(a)

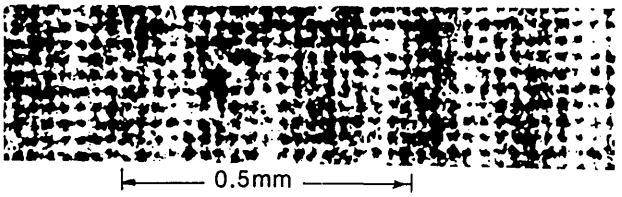

(b)

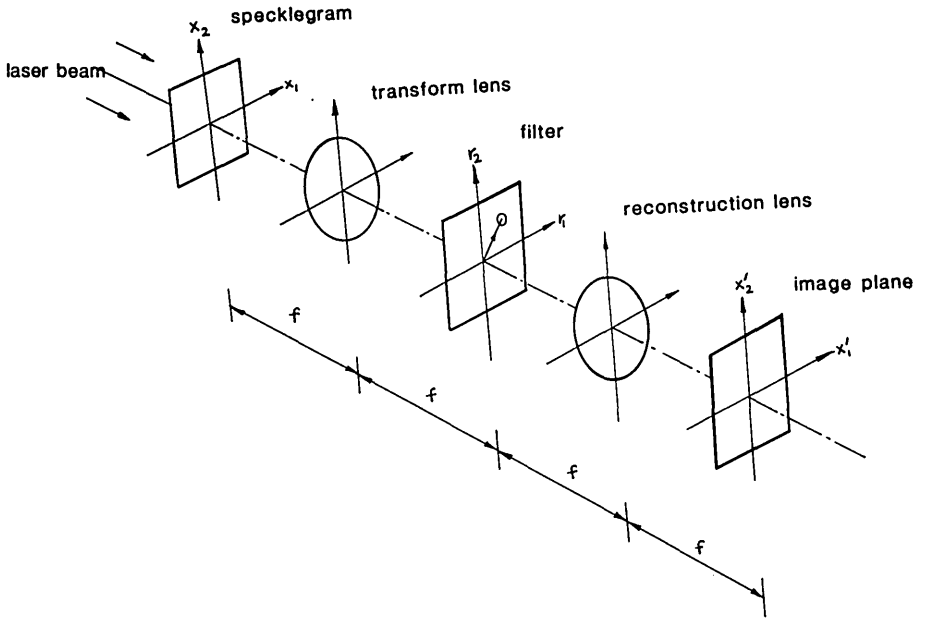

From Eqn. 13

Experimental

(c)

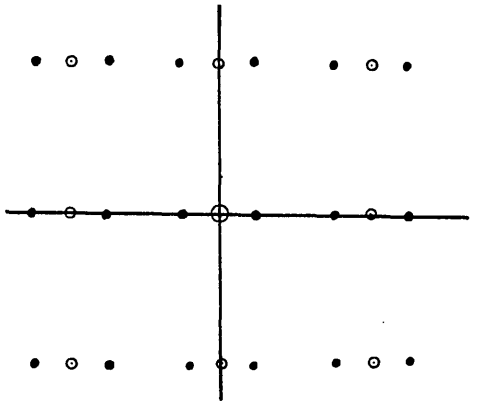

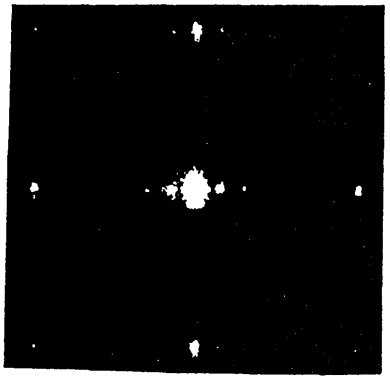

⊙ Due to the photoprinted cross grating

● Due to the projected line grating

Fig. 2. (a) Recorded combined moire gratings from the specimen surface. High frequency dots are the photoprinted cross gratings, and the low frequency dark and light bands are the projected gratings. (b) Schematic of the spatial filtering of combined moire and laser speckle grating recordings. (c) Diffraction spectrum on the focal plane of the transform lens. Note that the diffraction spots, say, along 45°, are too faint to be seen in the photograph.

where r_1 and r_2 are the coordinates of the spectral plane and $\otimes$ denotes the convolution operator. If $u = (r_1/\lambda f)$ and $v = (r_2/\lambda f)$ (f = focal length of the transform lens), then

$$T_g(u,v) = \int\int_{-\infty}^{\infty} t_g(x_1,x_2)\exp[-i2\pi(ux_1 + vx_2)]dx_1dx_2, \tag{12}$$

$$\begin{aligned}
T_g(u,v) &= \left[\delta(u,v) + \frac{1}{2}\delta\left(u-\frac{1}{p},v\right) + \frac{1}{2}\delta\left(u+\frac{1}{p},v\right)\right] \\
&\otimes \left[\delta(u,v) + \frac{1}{2}\delta\left(u,v-\frac{1}{q}\right) + \frac{1}{2}\delta\left(u,v+\frac{1}{q}\right)\right] \\
&\otimes \left[\delta(u,v) + \frac{1}{2}\delta\left(u-\frac{1}{\rho},v\right) + \frac{1}{2}\delta\left(u+\frac{1}{\rho},v\right)\right], \\
&= \left[\delta(u,v) + \frac{1}{2}\delta\left(u-\frac{1}{p},v\right) + \frac{1}{2}\delta\left(u+\frac{1}{p},v\right)\right. \\
&+ \frac{1}{2}\delta\left(u,v-\frac{1}{q}\right) + \frac{1}{2}\delta\left(u,v+\frac{1}{q}\right) \\
&+ \frac{1}{4}\delta\left(u-\frac{1}{p},v-\frac{1}{q}\right) + \frac{1}{4}\delta\left(u+\frac{1}{p},v-\frac{1}{q}\right) \\
&\left.+ \frac{1}{4}\delta\left(u-\frac{1}{p},v+\frac{1}{q}\right) + \frac{1}{4}\delta\left(u+\frac{1}{p},v+\frac{1}{q}\right)\right] \\
&\otimes \left[\delta(u,v) + \frac{1}{2}\delta\left(u-\frac{1}{\rho},v\right) + \frac{1}{2}\delta\left(u+\frac{1}{\rho},v\right)\right], \\
&= [A] \otimes [B], \\
&= [A] + [C] + [D],
\end{aligned} \tag{13}$$

where

$$\begin{aligned}
[C] = \left[\right.&\frac{1}{2}\delta\left(u-\frac{1}{\rho},v\right) + \frac{1}{4}\delta\left(u-\frac{1}{p}-\frac{1}{\rho},v\right) + \frac{1}{4}\delta\left(u+\frac{1}{p}-\frac{1}{\rho},v\right) \\
&+ \frac{1}{4}\delta\left(u-\frac{1}{\rho},v-\frac{1}{q}\right) + \frac{1}{4}\delta\left(u+\frac{1}{\rho},v+\frac{1}{q}\right) \\
&+ \frac{1}{8}\delta\left(u+\frac{1}{p}-\frac{1}{\rho},v-\frac{1}{q}\right) + \frac{1}{8}\delta\left(u-\frac{1}{p}-\frac{1}{\rho},v-\frac{1}{q}\right) \\
&\left.+ \frac{1}{8}\delta\left(u-\frac{1}{p}-\frac{1}{\rho},v+\frac{1}{q}\right) + \frac{1}{8}\delta\left(u+\frac{1}{p}-\frac{1}{\rho},v+\frac{1}{q}\right)\right],
\end{aligned}$$

and $[D]$ contains terms identical to $[C]$ with $1/\rho$ replaced by $-(1/\rho)$, and δ terms are the Dirac functions. This equation represents the diffraction spectrum shown in Fig. 2(c).

Similarly, the expression for $T_g'(u,v)$ corresponding to the deformed grating with the grating pitch denoted by p',q', and ρ' is

$$T_g'(u,v) = [A'] + [B'] + [C']. \tag{14}$$

From Eqs. (13) and (14), convolution (11) can be calculated. It contains $(27)^2$ terms, out of which only six are of interest from the point of view of surface displacement information contained in them. They are $\delta[u \pm (1/p),v]$, $\delta[u \pm (1/p'),v]$, $\delta[u \pm (1/\rho),v]$, $\delta[u \pm (1/\rho'),v]$, $\delta[u,v \pm (1/q)]$, and $\delta[u,v \pm (1/q')]$.

The reconstruction process after filtering is a second Fourier transform of the filtered information. When a mask with a small filtering hole is positioned at, say, $u = \pm(1/p)$ and $v = 0$, both $\delta[u \pm (1/p),v]$ and $\delta[u \pm (1/p'),v]$ will be reconstructed. The amplitude distribution on the image or reconstruction plane is

$$\begin{aligned}
E(-x_1,-x_2) &= \int\int_{\infty}^{\infty}\left[\delta\left(u-\frac{1}{p},v\right)\right. \\
&\left.+ \delta\left(u-\frac{1}{p'},v\right)\right]\exp[i2\pi(ux_1 + vx_2)]dudv, \\
&= \left[\exp\left(\frac{i2\pi x_1}{p}\right) + \exp\left(\frac{i2\pi x_1}{p'}\right)\right].
\end{aligned} \tag{15}$$

Then, the intensity distribution on the image plane is

$$\begin{aligned}
I_t = EE^* &= 2 + \exp\left[i2\pi x_1\left(\frac{1}{p}-\frac{1}{p'}\right)\right] + \exp\left[-i2\pi x_1\left(\frac{1}{p}-\frac{1}{p'}\right)\right] \\
&= 2\left[1 + \cos 2\pi x_1\left(\frac{1}{p}-\frac{1}{p'}\right)\right],
\end{aligned} \tag{16}$$

where $(\cdot)^*$ represents the complex conjugate. Equation (16) represents the fringe pattern due to deformation in the x_1-direction (isothetics or contours of u_1). Similarly, isothetics corresponding to u_2 and u_3 can be obtained by moving the mask with the filtering hole to positions $u = 0$; $v = \pm(1/q)$ and $u = \pm(1/\rho)$; $v = 0$, respectively. Equations governing the displacements are

$$u_1 = mp, \quad u_2 = m'q, \quad u_3 = \frac{m''\rho}{\tan\beta}, \tag{17}$$

where fringe orders $m,m',m'' = 0,\pm1,\pm2,\ldots$.

It is to be noted that in actual practice the photoprinted dot pattern on the specimen surface has an identical pitch in two orthogonal directions x_1,x_2, leading to the simplification $p = q$.

III. Laser Speckle Grating Method

The experimental setup used for this technique is essentially the same as the one used in the combined moire method. In this method, the specimen surface does not have photoprinted gratings, as in the previous case. Instead laser speckles formed due to the surface roughness of the specimen are used to measure in-plane deformations. Thus the process of specimen preparation is much simplified.

The optical arrangement described in the previous section is used to create a standing wave on the specimen surface. Simultaneously, a second optical field called the laser speckle field, which is a random interference pattern resulting from the mutual interference of numerous reflected wavelets from the specimen surface, forms in the entire volume in front of the surface. This laser speckle field has been exploited in recent years as an effective tool for measuring displacement and strain fields in solids and a velocity distribution in fluids. Thus the complex optical field on the surface consists of both projected gratings and laser speckles. Because the pitch of the grating is many times larger than the size of individual speckles, the recorded grating shows a structure that is made of many embedded speckles [Fig. 3(a)]. To facilitate the recording of the high frequency signals in this optical field, a mask with four circular apertures was used at the pupil plane of the lens.[12,13] This approach is shown to improve the quality of fringes in laser speckle photography. The mask creates a fine gratinglike structure within each recorded speckle.

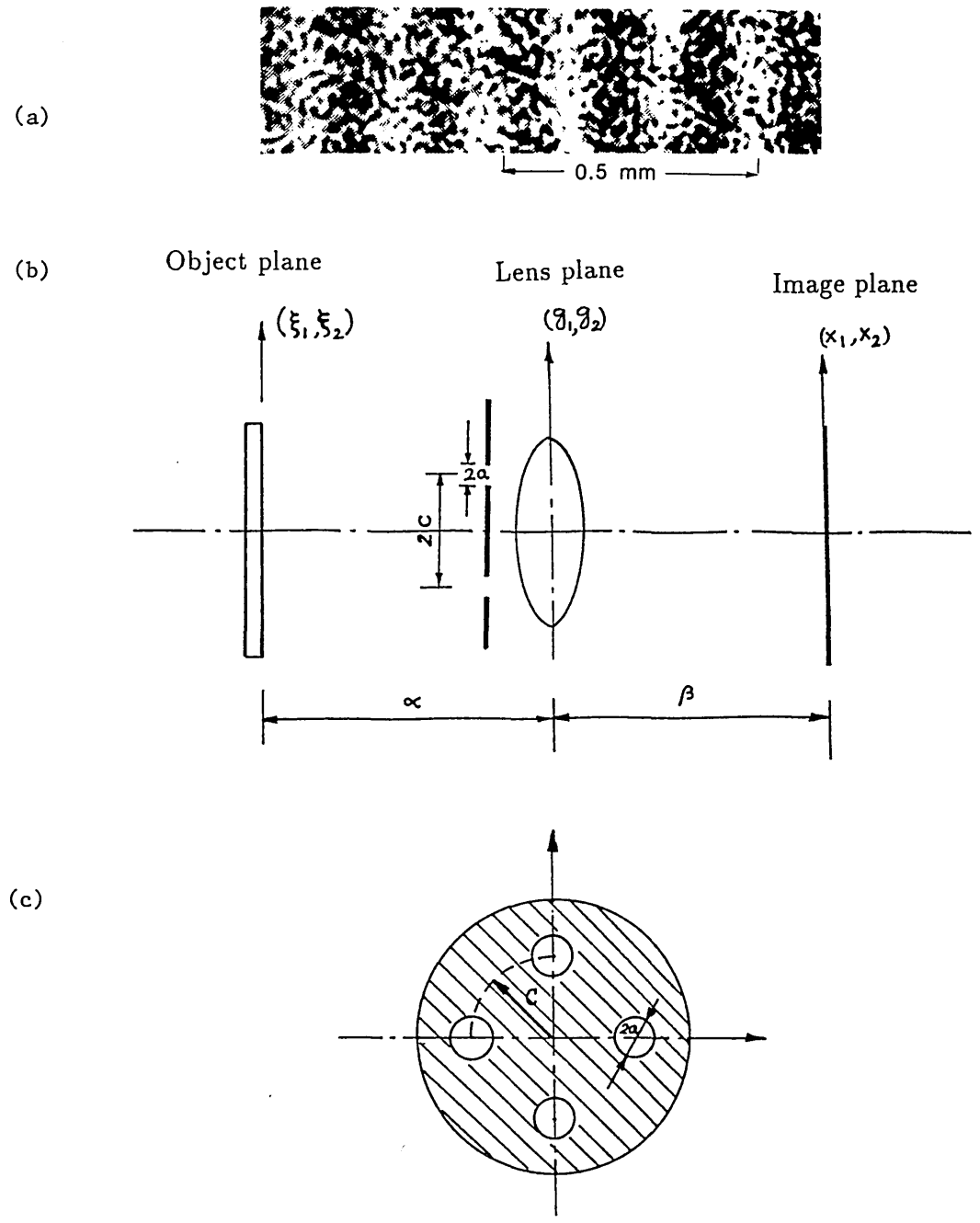

Fig. 3. (a) Laser speckle grating recording from the specimen surface. The high frequency random patterns are laser speckles with a gratinglike structure inside them. The low frequency light and dark bands are the projected gratings: (b) recording laser speckles using a four-aperture mask; (c) the four-aperture mask.

On deformation, the specimen's in-plane displacement (u_1 and u_2) is encoded into the displacement of the speckles, whereas its out-of-plane displacement is embedded in the distortion of the projected gratings. All this information can be delineated using an optical spatial filtering process. Analysis leading to the final realization of u_1, u_2, and u_3 contour maps can be done in two stages: (a) analysis of a single exposure speckle grating recording; (b) analysis of a double exposure speckle grating recording.

A. Single Exposure Speckle Grating Recording Using a Four-Aperture Mask

As mentioned earlier, the specimen plane (ξ_1,ξ_2 plane) contains interference fringes with embedded speckles. The process of coherent imaging is linear in amplitude[14] and can be expressed as

$$a_i(x_1,x_2) = a_o(\xi_1,\xi_2) \otimes h(x_1,x_2) = a_o\left(\frac{x_1}{M}, \frac{x_2}{M}\right) \otimes h(x_1,x_2), \qquad (18)$$

where a_i and a_o represent the random amplitude distribution on image and object planes, respectively. Parameter $h(x_1,x_2)$ is the impulse response of the diffraction-limited imaging system, M is the magnification factor, and $\otimes$ is the convolution operator. For a four-aperture mask used during recording, pupil function $P(g_1,g_2) = 1$ in the unshaded region and zero elsewhere [Figs. 3(b), (c)]. Hence

$$h(x_1,x_2) = \int\int_{-\infty}^{\infty} P(g_1,g_2)\exp\left[\frac{i2\pi}{\lambda\beta}(g_1x_1 + g_2x_2)\right]dg_1dg_2,$$

$$= FT[\mathrm{circ}\sqrt{(g_1^2+g_2^2)}]\left[\exp\left(\frac{i2\pi cx_1}{\lambda\beta}\right) + \exp\left(\frac{-2\pi cx_1}{\lambda\beta}\right) + \exp\left(\frac{i2\pi cx_2}{\lambda\beta}\right) + \exp\left(\frac{-i2\pi cx_2}{\lambda\beta}\right)\right],$$

$$= 8\pi a^2 \frac{2J_1\left(\frac{4\pi a\sqrt{x_1^2+x_2^2}}{\lambda\beta}\right)}{\left(\frac{4\pi a\sqrt{x_1^2+x_2^2}}{\lambda\beta}\right)} \times\left[\cos\left(\frac{2\pi cx_1}{\lambda\beta}\right) + \cos\left(\frac{2\pi cx_2}{\lambda\beta}\right)\right], \quad (19)$$

where J_1 represents the Bessel function of the first order. Other parameters β, c are constants associated with the recording system [Figs. 3(b), (c)]. Here the first term represents Airy's spot when $\sqrt{x_1^2 + x_2^2} \le 0.61(\lambda\beta/2a)$, and the second term denotes the high frequency carrier which is a gratinglike structure inside the speckles. A linearly processed specklegram can be expressed (after omitting the constant term) as

$$I(x_1,x_2) = a_i(x_1,x_2)a_i^*(x_1,x_2) \quad (20)$$

or

$$I(x_1,x_2) = \int_{-\infty}^{\infty} a_o\left(\frac{x_1'}{M},\frac{x_2'}{M}\right)a_o^*\left(\frac{X_1'}{M},\frac{X_2'}{M}\right)h(x_1-x_1',x_2-x_2') \times h(x_1-X_1',x_2-X_2')dx_1'dx_2'dX_1'dX_2'. \quad (21)$$

Here a^* is the complex conjugate of a. The frequency spectrum of $I(x_1,x_2)$ is obtained using the spatial filtering arrangement shown in Fig. 2(b). If $a_h(r_1,r_2)$ denotes the amplitude distribution on the frequency plane,

$$a_h(r_1,r_2) = \int\int_{-\infty}^{\infty} I(x_1,x_2)\exp\left[\frac{-i2\pi}{\lambda f}(r_1x_1 + r_2x_2)\right]dx_1dx_2, \quad (22)$$

and intensity $I_h(r_1,r_2)$ is given by

$$I_h(r_1,r_2) = |a_h(r_1,r_2)|^2. \quad (23)$$

Here Eq. (23) represents the halo on the frequency plane; the explicit formulation of the above is detailed in Refs. 12 and 15.

B. Double Exposure Speckle Grating Recording

To obtain whole field isothetics due a load increment $\Delta F = F_2 - F_1$, where F_1 and F_2 are the initial and final load levels, a double exposure scheme is used as follows:

(1) At load F_1, one of the diffraction orders used in creating the standing wave, say (-1), is allowed to illuminate the specimen surface. The corresponding speckle field recorded at load F_1 is

$$I_1 = A_{-1}(x_1 - u_1, x_2 - u_2), \quad (24)$$

where u_1 and u_2 are the in-plane displacements, A_{-1} is the intensity due to the (-1) diffraction order, and the coordinates are set on the deformed object.

(2) Then the load is increased to F_2, and both diffraction orders, $+1$ and -1, are allowed to impinge on the specimen surface simultaneously. This results in two overlapping but different speckle fields, $A_{+1}(x_1,x_2)$ and $A_{-1}(x_1,x_2)$. In addition to the formation of two speckle fields, the amplitude addition of two wavefronts results in a standing wave, as described previously. Thus the intensity recording corresponding to the second exposure is

$$I_2 = A_{-1}(x_1,x_2) + A_{+1}(x_1,x_2) + A_o\left(1 + \cos\frac{2\pi x_1}{\rho}\right), \quad (25)$$

where A_o is a constant. The linear processing of the doubly exposed film gives the transmittance of the speckle grating recording as

$$t = c_1 - c_2\tau(I_1 + I_2), \quad (26)$$

where c_1 and c_2 are constants and τ is the exposure time. The constant term can be neglected because it represents the image of the point source during filtering. Also, A_{+1} does not contribute toward any displacement information, since it does not have a corresponding speckle pattern in the first exposure.

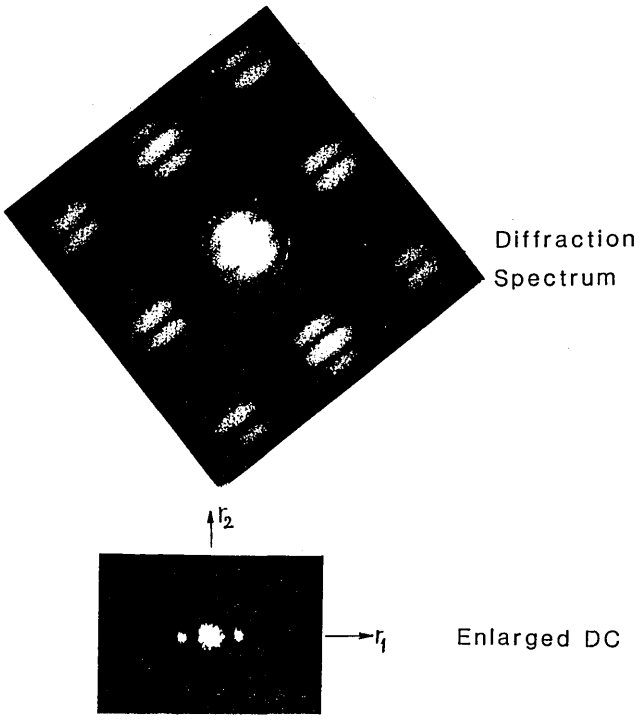

Fig. 4. Diffraction spectrum of a laser speckle grating recording. The enlarged dc region clearly shows two diffraction spots on either side of the dc due to the lower frequency projected gratings.

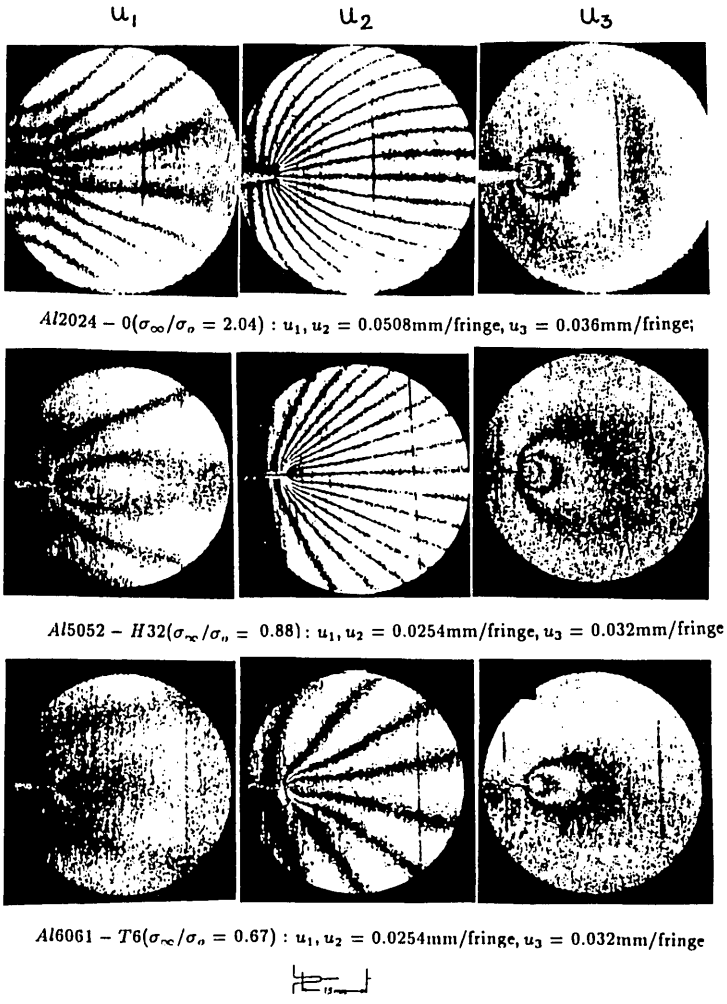

Fig. 5. Isothetics of u_1, u_2, and u_3 displacement components near a plastically deformed crack tip in three types of aluminum alloy of different strain hardening characteristics. Fringes were obtained using the combined moire method.

Assuming that displacements u_1 and u_2 are slowly varying functions of x_1 and x_2,

$$
\begin{aligned}
FT(t) &= FT\left[A_o\left(1+\cos\frac{2\pi x_1}{\rho}\right)\right] \\
&+ \int\int_{-\infty}^{\infty} A_{-1}(x_1,x_2)\exp\left[\frac{-i2\pi}{\lambda f}(r_1x_1+r_2x_2)\right]dx_1dx_2 \\
&+ \exp\left[\frac{i2\pi}{\lambda f}(r_1u_1+r_2u_2)\right]\int\int A_{-1}(x_1-u_1,x_2-u_2) \\
&\times \exp\left\{\frac{-i2\pi}{\lambda f}[r_1(x_1-u_1)+r_2(x_2-u_2)]\right\}dx_1dx_2 \\
&= A_o\left[\delta(u,v)+\frac{1}{2}\delta\left(u-\frac{1}{\rho},v\right)+\frac{1}{2}\delta\left(u+\frac{1}{\rho},v\right)\right] \\
&+ \left\{1+\exp\left[\frac{i2\pi}{\lambda f}(r_1u_1+r_2u_2)\right]\right\}FT[A_{-1}(x_1,x_2)], \qquad (27)
\end{aligned}
$$

where $u = (r_1/\lambda f)$ and $v = (r_2/\lambda f)$.

In the above equation, the first term is contributed by the projected grating, whereas the second is due to laser speckles (Fig. 4). The in-plane displacement information is embedded in the second term. By positioning a mask with a filtering hole along the r_1 (or r_2) axis, u_1 (or u_2) isothetics can be obtained on the reconstruction plane. Displacements are governed by

$$
\begin{aligned}
\mathbf{u}\cdot\mathbf{d} &= \left(\frac{n+1}{2}\right)\lambda f \quad \text{for dark fringes,} \\
&= n\lambda f \quad \text{for light fringes,}
\end{aligned}
$$

where

$$
\begin{aligned}
\mathbf{u} &= u_1\mathbf{e}_1 + u_2\mathbf{e}_2, \\
\mathbf{d} &= r_1\mathbf{e}_1 + r_2\mathbf{e}_2. \qquad (28)
\end{aligned}
$$

To extract the out-of-plane displacement information u_3, the speckle grating recording is filtered along with a master grating as was done in the combined moire method with a filtering hole positioned at $(r_1/\lambda f) = \pm(1/\rho)$.

IV. Results and Discussion

The two methods described were implemented to study deformations occurring near an elastoplastically deformed crack tip. The specimens were made of different aluminum alloys with different work hardening characteristics. They were single-edge-notch fracture specimens and were subjected to far field uniform tension. In the combined moire method a 40-dot/mm grating was photoprinted on the specimen surface. A line grating pattern was projected on the specimen

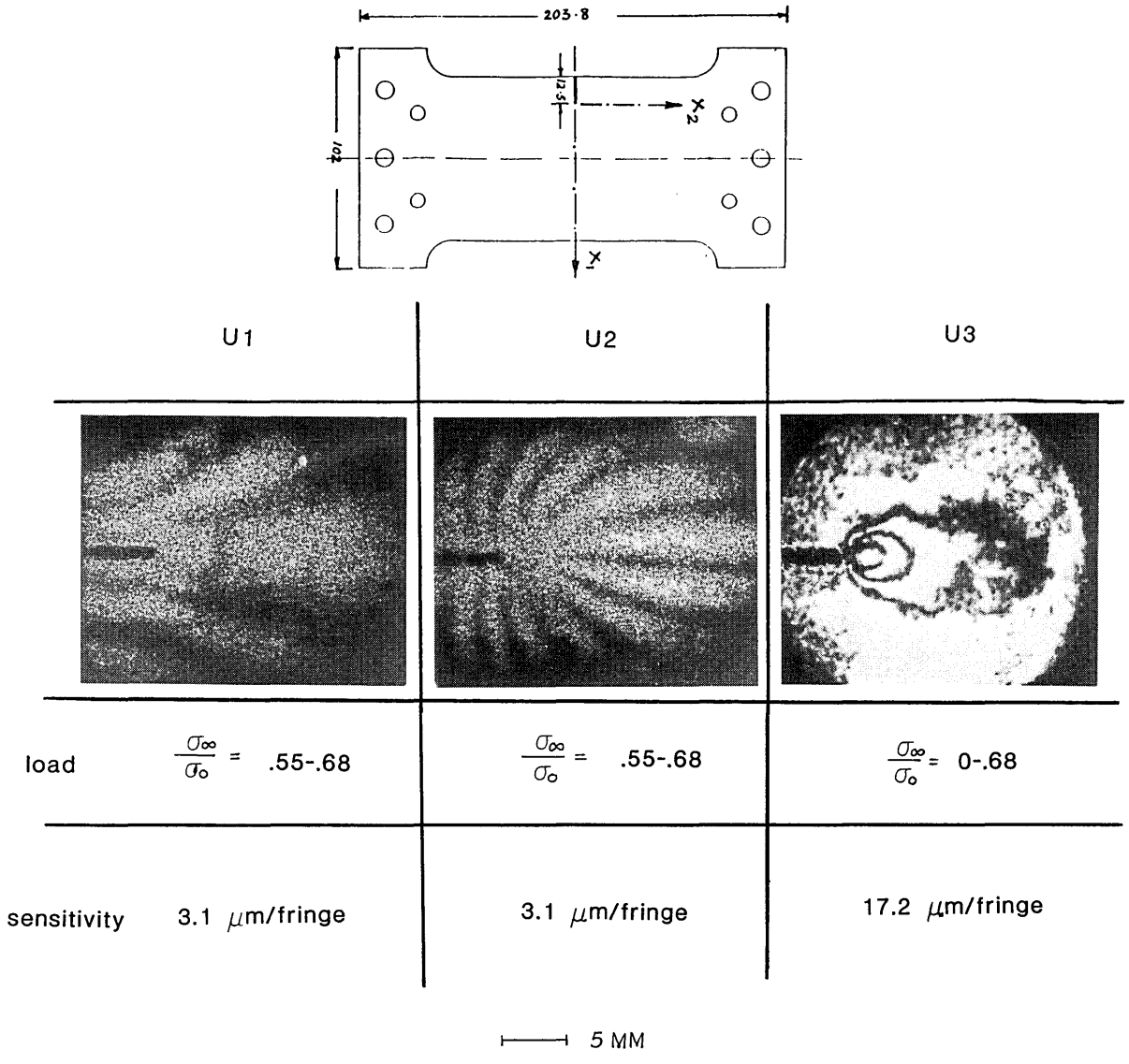

Fig. 6. Isothetics of u_1, u_2, u_3 displacement components near a deformed crack tip in a single edge notch fracture specimen obtained using the laser speckle grating method.

surface with the angle of projection ranging from 72° to 76°. Figure 2(c) shows the diffraction spectrum observed during the spatial filtering of the recorded grating. On filtering the essential frequencies, the isothetics of u_1,u_2, and u_3 are generated on the image or reconstruction plane of the filtering setup. Figure 5 shows typical fringe patterns observed by using this technique.

The speckle grating method requires no special surface preparation of the specimen but a spray of flat white paint on the surface to help improve the brightness of the speckle field. The typical diffraction halo of a double exposure recording is shown in Fig. 4. By selectively filtering the essential frequencies, isothetic maps, as shown in Fig. 6, are obtained. It should be noted that the sensitivity of in-plane fringes is an order higher than u_3 fringes unlike in the combined moire method where the sensitivities of all three fringe patterns are of the same order. However, for elastoplastic deformation studies close to the crack tip, the speckle-grating method has a drawback because it suffers from decorrelation effects[15] due to the large displacements and surface texture changes. This effect is evident near the immediate vicinity of the crack tip of the in-plane fringes shown in Fig. 6.

The work was performed in the Laboratory for Experimental Mechanics Research, SUNY at Stony Brook, as part of H.V.T.'s doctoral research. The financial support for the research by the ONR Mechanics Division through contract N0001482K0566 (Y. Rajapakse, Scientific Officer) and the NSF Solid and Geo-Mechanics program grant MEA8403912 to F.P.C. is acknowledged.

References

1. F. P. Chiang, "Moire Methods in Strain Analysis," in *Manual of Experimental Stress Analysis Techniques*, A. S. Kobayashi, Eds. (SESA, Brook Field Center, CT, 1978).
2. F. P. Chiang, "A New Family of 2-D and 3-D Experimental Stress Analysis Techniques Using Laser Speckles," S. M. Arch. **3,** 27–58 (1978).
3. A. J. Rosakis, "Analysis of Optical Shadow Spot Method for a Tensile Crack in a Power Law Hardening Material," J. Appl. Mech. **50,** 777–782 (1983).
4. A. J. Rosakis and L. B. Freund, "Optical Measurement of the Plastic Strain Concentration at a Crack Tip in a Ductile Steel Plate," J. Eng. Mater. Technol. **104,** 115–119 (1982).
5. F. D. Adams and G. E. Maddux, "Synthesis of Holography and Speckle Photography to Measure 3-D Displacements," Appl. Opt. **13,** 219 (1974).
6. F. P. Chiang, Q. B. Li, and J. B. Chen, "Holo-speckle Interferometry," in *Proceedings, SESA International Congress on Experimental Mechanics*, Montreal (1984).
7. X. P. Wu and F. P. Chiang, "Sandwich Holo-speckle Interferometry for 3-D Displacement Determination," at *Twenty-Ninth Annual International Technical Symposium on Optical and Electrooptical Engineering*, San Diego (SPIE, 1985).
8. G. J. Jaisingh, "Studies in One-Beam Laser Speckle Interferometry," Ph.D. Dissertation, Department of Mechanical Engineering, SUNY, Stony Brook (1979).
9. R. P. Ketan and F. P. Chiang, "A General Analysis of Projection Moire Methods," in *Proceedings, Fifteenth Midwestern Mechanics Conference*, Chicago Circle (1977).
10. F. P. Chiang and R. C. Williams, Jr., "Simultaneous Generation of 3-D Displacement Contours of a Fracturing Specimen Using Moire," Eng. Fract. Mech. **22,** 731–735 (1985).
11. F. P. Chiang, "Techniques of Optical Spatial Filtering Applied to Processing of Moire Fringe Patterns," Exp. Mech. **6,** 523–526 (1979).
12. F.-P. Chiang and R. P. Khetan, "Strain Analysis by One-Beam Laser Speckle Interferometry. 2: Multiaperture Method," Appl. Opt. **18,** 2175–2186 (1979).
13. F.-P. Chiang and D. W. Li, "Diffraction Halo Functions of Coherent and Incoherent Random Speckle Patterns," Appl. Opt. **24,** 2166–2171 (1985).
14. J. W. Goodman, *Introduction to Fourier Optics* (McGraw-Hill, New York, 1968).
15. D. W. Li, "Study of Laser and White-Light Speckle Methods for Deformation Measurement," Ph.D thesis, SUNY, Stony Brook (1985).